Research Article – Vol. 02, Issue 01, No. 08

Advanced in Engineering and Intelligence Systems

Journal Web Page: https://aeis.bilijipub.com

Performance improvement of a flash-binary geothermal power system using zeotropic working fluid; A comprehensive exergoeconomic analysis and optimization

Seyed Sajad Mosavias[1] , Ali Dezhdar[2,3,*] Sajjad Keykhah[1] , Ehsan Farhadi[1], Mojtaba Nedaei[4,5]

[1] *Department of Mechanical Engineering, Dezful Branch, Islamic Azad University, Dezful, Iran*
[2] *Young Researchers and Elite Club, Dezful Branch, Islamic Azad University, Dezful, Iran*
[3] *Kimia Andimeshk Petrochemical Industries Company, Khuzestan-Iran*
[4] *Department of Management and Engineering, University of Padua (Padova), Vicenza, Italy*
[5] *University of Warsaw, Warsaw, Poland*

Highlights

- *A flash-binary geothermal-based system is proposed for power generation.*
- *Zeotropic mixtures as the working fluid are used for performance improvement.*
- *Thermodynamic, exergoeconomic, and optimization assessments were performed.*
- *The system led to generating 3841 kW net power with 61.09% exergetic efficiency.*
- *The optimum payback and exergetic efficiency were obtained to be 3.26 years and 62.15%, respectively.*

Article Info

Received: 05 March 2023
Received in revised: 27 March 2023
Accepted: 26 March 2023
Available online: 28 March 2023

Keywords

Geothermal flash-binary system
Zeotropic mixture
Exergoeconomic analysis;
Net present value;
Multi-objective optimization

Abstract

In this paper, a geothermal system is combined with an organic Rankine cycle to generate power. The zeotropic mixture is utilized to improve the organic Rankine cycle performance. The mass, energy, exergy, and exergoeconomic analysis is applied to evaluate the proposed system performance, in which the system led generated 3841 kW net power with 61.09% exergetic efficiency and 3.55 years of payback period. Then, a parametric study is performed to obtain the effect of vapor generator temperature and zeotropic mixture's mass fraction on the proposed system's main performance criteria. Based on the parametric study results, the mass fraction variation influences the net power generation, energy and exergetic efficiencies, and the payback period is higher than the evaporation temperature in the vapor generator unit while, the exergy destruction is influenced by the evaporation temperature higher than the zeotropic mixture mass fraction. Also, the net present value is estimated for three different geofluid and electricity sale prices. Increasing the electricity price about 22% with the same geofluid price decreases the payback period by about 23% and improves the system profit by about 54.7%. Finally, applying a multi-objective optimization refers to obtaining the payback and exergetic efficiency by about 3.26 years and 62.15%, respectively.

Nomenclature

c	*Cost per exergy unit* $[\$.GJ^{-1}]$	t	*Time* $[s]$
CRF	*Capital Recovery Factor*	T	*Temperature* $[K]$
$Cond$	*Condenser*	Tur	*Turbine*
e	*Exergy* $[kJ.kg^{-1}]$	VG	*Vapor Generator*
$\dot{E}$	*Exergy flow* $[kW]$	$\dot{W}$	*Power* $[kW]$
EV	*Expansion Valve*	Z	*Investment cost of components* $[\$]$

* Corresponding Author: Ali Dezhdar
Email: ali.dezhdar@gmail.com

$\dot{E}x$	*Exergy flow* $[kW]$	***Subscript and abbreviations***	
h	*Enthalpy* $[kJ.kg^{-1}]$	*cr*	*Critical*
K	*Interest rate [%]*	*D*	*Destruction*
$\dot{m}$	*Mass Flow Rate* $[kg.s^{-1}]$	*Elec*	*Electrical*
$M\ M$	*Molar Mass* $[g.mole^{-1}]$	*en*	*Energy*
Mix	*Mixer*	*ex*	*Exergy*
NPV	*Net Present Value* [$]	*in*	*Inlet*
O&M	*Operation and Maintenance*	*is*	*Isentropic*
OFC	*Organic Flash Cycle*	*PPT*	*Pinch Point Temperature [K]*
ORC	*Organic Rankine Cycle*	*sep*	*Separator*
P	*Pressure [kPa]*	*out*	*Outlet*
PEC	*Purchased Equipment Cost [$]*	0	*Dead State*
Pu	*Pump*	1,2,3, …	*State Point*
Q	*Heat* $[kJ]$	***Greek symbols***	
s	*Entropy* $kJ.kg^{-1}.K^{-1}$	η	*Efficiency*
ST	*Steam Turbine*	φ	*Maintenance Factor*

1. Introduction

Fossil fuels prepare over 60-70% of the power system's required energy to supply power demand [1]. These fuel reservoirs are limited and contain environmental pollution such as global warming, CO2 emission, etc [2]. Hence, the researchers introduce renewable energy reservoirs as a substitution of fossil fuels for power systems. Solar, wind, ocean waves, and geothermal energies are the most famous renewable energies. But, except for the geothermal system, all these energies performance is highly influenced by climate conditions[3], [4]. Therefore, the geothermal energy can provide sustainable resources for power systems. The geothermal reservoir with a temperature range of below 90 ˚C is considered a low-temperature reservoir, between 90 to 150 ˚C is a moderate-temperature reservoir, and higher than 150 ˚C is a high-temperature reservoir [5]. Primary geothermal fluid was dry-steam, and this kind of geothermal fluid is sacred, while most of the discovered geothermal reservoirs were moisture-steam [6]. The use of appropriate subsystems is more critical to achieve high performance and lower costs in renewable renewable-based power systems. Geothermal energy is a heat source in many countries, but it has never been investigated for the implementation of a poly-generation plant, containing branched GAX cycle and electrolysis. In [26] a high-efficiency multigeneration system with Sabalan geothermal power system (Savalan) including a single flash cycle, a branched GAX cycle and an electrolysis is represented and investigated from a thermodynamic and exeroeconomic point of view. Finally, a two-objective optimizing by total unit cost of product (TUCP) and energy performance as objectives is used achieving the optimal conditions. Luo et al. [7] compared binary and single-flash geothermal power system performance from exergetic assessment at China's six different geothermal power systems. Their results indicated that the binary system presented a higher performance for geothermal fluid which contained less than 130 ˚C, and the single-flash system is proper for higher temperature geothermal fluid. Yari [8] investigated the different configurations of the binary high-temperature geothermal system from energy approach and showed that the flash-binary arrangement presented higher performance. Also, higher performance was achievable by adding an ORC subsystem with a regenerative and internal heat exchanger. Pasek et al. [9] studied a flash-binary geothermal system, which supplied an ORC subsystem. They examined different organic substances to select the best working fluid. Their results revealed that the i-Pentane provides the highest net output power and thermal efficiency. Mosharavati et al. [10] compared two configurations of a flash-binary geothermal system. The geofluid extracted and ran an ORC and absorption cooling system as a subsystem in the first proposed scenario. In the second scenario, the geofluid exited at two stages. The first one is the same as the first proposed scenario. The second part referred to reverse osmosis unit and a turbine applied at reverse osmosis brined water. Their results indicated that the second scenario produced 70.85 kW net power and presented 20.16% exergetic efficiency more than the first scenario, while the first scenario contained lower electricity cost rate. Mosaffa and Zareei [11] presented different arrangements for organic flash cycle, and they studied the heat recovery from the flash-binary plant. According to results, use of 2-phase expander along with a single-flash organic flash cycle improved the net power about 36.7%. Seyyedvalilu et al. [12] proposed three different hybrid

system configurations driven by the binary geothermal system and compared their performance from exergy and exergoeconomic assessment. Their results revealed that the double-effect absorption heat transformer system prepared 57.38% exergetic efficiency with sum unit cost production of 0.04636 $/kWh. Guzovic et al. [13] studied a moderate-temperature geothermal power system performance by adding subsystems in Croatia. They compared utilizing an ORC and a Kalina cycle as geothermal subsystems and showed that using the ORC system represented 2225 kW power while using the Kalina cycle represented 2101 kW power. The ORC subsystems contained a phase-change procedure in the heat exchanger system, which happens in a fixed temperature and considers significant exergy destruction and temperature mismatch. For minimizing the exergy destruction, the zeotropic fluids utilization as the working fluid of ORC subsystems can be helpful [14]. The zeotropic fluids include two organic fluids that have various vaporization temperatures. So, during the phase-change, the temperature doesn't hold constant, and the exergy destruction and the temperature mismatch in the heat exchanger considerably decrease [15]. Li et al. [16] studied an ORC system, where pure fluids are compared with zeotropic fluids. Their obtained results indicated that efficiency of their suggested system considerably is improved by using the zeotropic fluids with an internal heat exchanger. Wang et al. [17] investigated the solar Rankine cycle, where various zeotropic fluids and mass fractions are considered. They showed that the system performance by adding superheating and internal heat exchanger improved considerably. Zhao et al. [18] represented an experimental comparison of the zeotropic and pure substance performance at the ORC system. They showed that the zeotropic fluid of R245fa-R152a with the mass fraction of 0.7-0.3 represent higher thermal performance compared to pure R245fa. proposes a new hybrid system based on a binary-geothermal system to generate power, cooling capacity, freshwater, and hydrogen. This system includes an internal integration of the organic Rankine cycle and ejector refrigeration cycle with zeotropic working fluids, proton exchange membrane electrolyzer, and reverse osmosis desalination unit. The system is analyzed by developing a precise model in the Matlab software, and then a multi-objective grey wolf optimization is employed to optimize the proposed system performance. The net present value, payback period, and sum unit cost of products are considered the system's economic performance criteria to study the system's feasibility for investment. Results indicate that the Isobutene-R114 provides the best net output power, and the R12-R114 combination has the best cooling performance. Also, the R12-R114 reports the best overall performance as the organic Rankine cycle working fluid.

1.1. Main contribution and novelties

As visualized in prior studies, the flash-binary system was a hot-spotted configuration of the geothermal power system. Also, the ORC system was a proper choice to restore the wasted energy of the geothermal power system, especially with zeotropic working fluid. Hence, this paper proposes a single flash-binary geothermal power system accompanying an ORC subsystem to produce power from a moderate-temperature geothermal. The energy, exergy, and exergoeconomic study and analysis is conducted to evaluate the proposed system's performance. Also, the following novelties are considered in this paper:

- Selection of zeotropic solution as ORC subsystem to improve its performance.
- Studying different zeotropic solutions and selecting Neopentane and R124 as dry-type ORC working fluids that are no need to be superheated.
- Conducting a parametric study to investigate the effect of some main parameters on system performance.
- Consider three different scenarios to apply the net present value and evaluate the profitability and payback period.

The rest of this paper can be categorized as follows. In section 2, we describe the proposed system. In Section 3, the mass, energy, exergy and exergeoeconomic equation that governs all components is discussed and mathematical modeling is expressed. In section 4 the results and discussion are presented and Section 5 Comprehensive energy, exergy, and exergoeconomic analysis have been performed to evaluate the proposed system performance. The conclusion is also stated in section 6.

2. System description

Fig. 1 shows the schematic diagram of proposed system. The geofluid is extracted from underground and enters the expansion valve. 1 (state. 1). The geofluid becomes a two-phase fluid in the expansion valve and is referred to separator tank (state. 2). Inside the separator tank, the vapor part of geofluid is extracted and led to steam turbine (state. 3), and the liquid portion is led to vapor generator unit (state. 4). The steam is expanded in the turbine and generates power then enters Cond. 1 unit to cool down (state. 5). In the Cond. 1 unit, the geofluid becomes saturated liquid and is led to the mixer unit (state. 6). On the other hand, the separator outlet liquid part enters the ORC vapor generator unit and transfers heat to the ORC subsystem. Then, it crosses the expansion valve. 2 (state. 8). In the expansion valve. 2, the geofluid turns into

two-phase fluid and enters the mixer. The expansion valve. 2 and Cond. 1 outlet flows are mixed in the mixer and brined underground (state. 9). In the ORC subsystem, the zeotropic solution, in which the physical properties of the utilized substances are demonstrated in Table 1, reaches a saturated vapor state and enters the ORC turbine (state. 10). Then, it is expanded in the ORC turbine and generates power. The ORC turbine outlet flow is led to Cond. 2 unit (state. 11), and cooling process is conducted on it. The zeotropic solution leaves the Cond. 2 unit at a saturated liquid state and enters the pump (state. 12). The zeotropic solution is pressurized in the pump to reach the vapor generator inlet pressure and then enters the vapor generator to complete the cycle (state. 13).

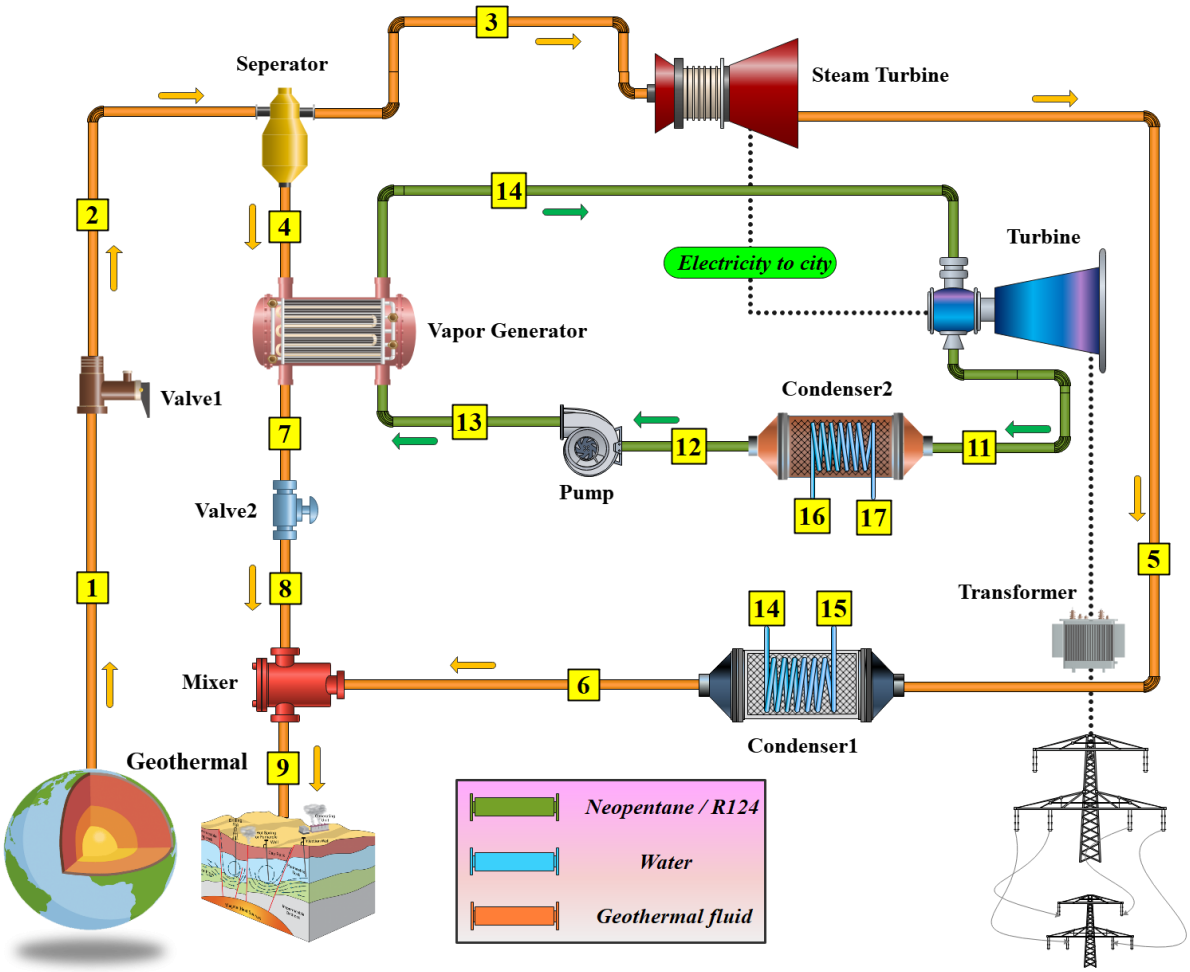

Fig. 1. Schematic diagram of the proposed system.

Table 1. The main characteristics of the fluids employed in this work.

Fluid	**T_{cr} [K]**	**P_{cr} [kPa]**	**MM [g, mol^{-1}]**
Neopentane	433,74	3196	72,15
R124	395,43	3624,30	136,48

The following assumptions are considered to analyze the proposed system:

1. All components are in steady state [19].
2. Changes in kinetic and potential energies are negligible [19].
3. The pressure drop in cycle pipe line and heat exchangers does not considered [19].
4. All components are adiabatic and there is no heat lost to ambient [19].
5. All turbines and pumps work at certain isentropic efficiencies [20].
6. Throttling process at expansion valve assumed constant enthalpy [21].

Also, some main input parameters for the steady-state simulation is tabulated at Table 2

Table 2. Some main input parameters and assumptions.

Parameter	symbol	Value	unit
Reference temperature	T_0	293,15	[K]
Reference pressure	P_0	101	[kPa]
Geothermal fluid mass flow rate	$\dot{m}_{(1)}$	30	[kg, s^{-1}]
Geothermal fluid enthalpy	$h_{(1)}$	1000,	[kJ, kg^{-1}]
Geothermal fluid pressure	$P_{(1)}$	120000000(	[kPa]
Steam turbine inlet pressure	$P_{(2)}$	550	[kPa]
Steam turbine isentropic efficiency	$\eta_{is.ST}$	85,	[%]
ORC turbine isentropic efficiency	$\eta_{is.Tur}$	85,	[%]
ORC pump isentropic efficiency	$\eta_{is.Pump}$	85,	[%]
Pinch point temperature difference of the condenser	$\Delta T_{PPT.Cond}$	10	[K]
Pinch point temperature difference of the vapor generator	$\Delta T_{PPT.VG}$	15,	[K]

3. Mathematical modeling

In this section, the mass, energy, exergy and exergoeconomic equation that governed on all component are discussed.

3.1.Mass and energy balance

The mass and energy1balance relations at the1steady-state with neglecting the kinetic1and1potential energies change, could be written as [22]:

$$\sum \dot{m}_{in} = \sum \dot{m}_{out} \quad (1)$$

$$\dot{Q} - \dot{W} = \sum \dot{m}_{out} h_{out} - \sum \dot{m}_{in} h_{in} \quad (2)$$

$\dot{m}$ is the mass flow rate of working fluid, $\dot{Q}$ and $\dot{W}$ are the net rate of inlet heat and output work, respectively and h indicate the specific enthalpy.

3.2. Exergy balance

The exergy balance at the steady steady-state is given by [22]:

$$\dot{E}_Q - \dot{W} = \sum \dot{m}_{out} e_{out} - \sum \dot{m}_{in} e_{in} + \dot{E}_D \quad (3)$$

where $\dot{E}_D$ determines the exergy destruction rate. Also, $\dot{E}_Q$ the net exergy transfer that can be calculated by [22]:

$$\dot{E}_Q = \sum \dot{Q} \left(1 - \frac{T_0}{T}\right) \quad (4)$$

in which T denotes the temperature. As well, T_0 refers to the dead-state temperature. The exergy low can be presented as follows [22]:

$$e = h - h_0 - T_0(s - s_0) \quad (5)$$

in which, s denotes the specific entropy. Furthermore, the mass, energy and exergy balance of each component for considered cases of study are illustrated at Table 3.

Table 3. The mass, energy, and exergy balance equations of proposed system components.

Component	Mass balance	Energy balance	Exergy balance
Expansion valve 1	$\dot{m}_1 = \dot{m}_2$	$\dot{m}_1 h_1 = \dot{m}_2 h_2$	$\dot{E}_D^{EV,1} = \dot{E}_1 - \dot{E}_2$
Separator	$\dot{m}_2 = \dot{m}_3 + \dot{m}_4$	$\dot{m}_2 h_2 = \dot{m}_3 h_3 + \dot{m}_4 h_4$	$\dot{E}_D^{Sep} = \dot{E}_2 - (\dot{E}_3 + \dot{E}_4)$
Steam turbine	$\dot{m}_3 = \dot{m}_5$	$\dot{W}_{ST} = \dot{m}_3 h_3 - \dot{m}_5 h_5 = (\dot{m}_3 h_3 - \dot{m}_5 h_{5s})\eta_{is,ST}$	$\dot{E}_D^{ST} = (\dot{E}_3 - \dot{E}_7) - \dot{W}_{ST}$
Condenser 1	$\dot{m}_{14} = \dot{m}_{15}, \dot{m}_5 = \dot{m}_6$	$\dot{Q}_{Cond,1} = \dot{m}_5 h_5 - \dot{m}_6 h_6 = \dot{m}_{15} h_{15} - \dot{m}_{14} h_{14}$	$\dot{E}_D^{Cond,1} = (\dot{E}_5 - \dot{E}_6) - (\dot{E}_{15} - \dot{E}_{14})$
Mixer	$\dot{m}_9 = \dot{m}_6 + \dot{m}_8$	$\dot{m}_9 h_9 = \dot{m}_6 h_6 + \dot{m}_8 h_8$	$\dot{E}_D^{Mixer} = (\dot{E}_6 + \dot{E}_8) - \dot{E}_9$
Expansion valve 2	$\dot{m}_7 = \dot{m}_8$	$\dot{m}_7 h_7 = \dot{m}_8 h_8$	$\dot{E}_D^{EV,2} = \dot{E}_7 - \dot{E}_8$
Vapor generator	$\dot{m}_4 = \dot{m}_7, \dot{m}_{13} = \dot{m}_{10}$	$\dot{Q}_{VG} = \dot{m}_4 h_4 - \dot{m}_7 h_7 = \dot{m}_{10} h_{10} - \dot{m}_{13} h_{13}$	$\dot{E}_D^{VG} = (\dot{E}_4 - \dot{E}_7) - (\dot{E}_{10} - \dot{E}_{13})$
Turbine	$\dot{m}_{10} = \dot{m}_{11}$	$\dot{W}_{Tur} = \dot{m}_{10} h_{10} - \dot{m}_{11} h_{11} = (\dot{m}_{10} h_{10} - \dot{m}_{11} h_{11s})\eta_{is,Tur}$	$\dot{E}_D^{Tur} = (\dot{E}_3 - \dot{E}_7) - \dot{W}_{Tur}$
Condenser 2	$\dot{m}_{11} = \dot{m}_{12}, \dot{m}_{16} = \dot{m}_{17}$	$\dot{Q}_{Cond,2} = \dot{m}_{11} h_{11} - \dot{m}_{12} h_{12} = \dot{m}_{17} h_{17} - \dot{m}_{16} h_{16}$	$\dot{E}_D^{Cond,2} = (\dot{E}_{11} - \dot{E}_{12}) - (\dot{E}_{17} - \dot{E}_{16})$
Pump	$\dot{m}_{12} = \dot{m}_{13}$	$\dot{W}_P = \dot{m}_{13} h_{13} - \dot{m}_{12} h_{12} = (\dot{m}_{13} h_{13s} - \dot{m}_{12} h_{12}) / \eta_{is,Pump}$	$\dot{E}_D^{Pump} = \dot{W}_{Pump} - (\dot{E}_{13} - \dot{E}_{12})$

3.3. Exergoeconomic analysis

The exergy and energy analysis represent the thermodynamical statement of systems performances. In reality, the energy and exergy approaches do not illustrate the appropriate definition of proposed system performance so, the economic analysis along with exergy analysis perform a brief statement of system performances and all power systems required a exergoeconomic analysis to represent a real statement of systems performance. Therefore, at this study, exergoeconomic analysis was performed. In this section, we represented a comprehensive exergoeconomic analysis of proposed system. The exergoeconomic analysis is based on applying economic equations on exergy balance for each component. The cost-balancing equation can be expressed as [23]:

$$\dot{C}_P = \dot{C}_F + \dot{C}^{CL} + \dot{C}^{OM} \quad (6)$$

where

$$\dot{C} = c\dot{E} \quad (7)$$

$\dot{C}_P$ is total cost of system product, $\dot{C}_F$ is the total cost of production, $\dot{C}^{CL}$ is the fixed-cost associated with fixed investment and $\dot{C}^{OM}$ represent the operation and maintenance cost. In order to evaluate the unit cost of input and output exergy flows ($\dot{E}x_{in}$,$\dot{E}x_{out}$), the power ($\dot{E}x_w$) and

heat transfer ($\dot{E}x_q$), the following equations are utilized [24]:

$$\dot{C}_{in} = c_{in}\dot{E}_{in} = c_{in}(\dot{m}_{in}e_{in}) \quad (8)$$

$$\dot{C}_{out} = c_{out}\dot{E}_{out} = c_{out}(\dot{m}_{out}e_{out}) \quad (9)$$

$$\dot{C}_w = c_w\dot{E}_w = c_w(\dot{m}_w e_w) \quad (10)$$

$$\dot{C}_q = c_w\dot{E}_q = c_q(\dot{m}_q e_q) \quad (11)$$

in which, the c_{in}, c_{out}, c_w and c_q are the average costs in the exergy unit ($\$ /MWh$).

Also, the cost of exergy destruction of each component can be expressed as [23]:

$$\dot{C}_{D,i} = c_{P,i}\dot{E}_{D,i} \ \ (if\ \dot{E}_{F,i} = constant\ value) \quad (12)$$

The total cost for component *i* is sum of the capital cost ($\dot{Z}^{CL}$) and the operation and maintenance ($\dot{Z}^{OM}$) cost [23]:

$$\dot{Z}_i = \dot{Z}^{CL} + \dot{Z}^{OM} \quad (13)$$

The total cost of each unit can be evaluated as [24]:

$$\dot{Z}_i = \frac{CRF \times \varphi}{N \times 3600} \times Z_i \quad (14)$$

which Z_i is the purchasing fixed cost of system components, N is the annual runtime of each component and assumed 7000 hours, φ is the maintenance factor and is 1.06 and CRF is the capital recovery factor, which can be calculated from following equation [24]:

$$CRF = \frac{K(1+K)^n}{(1+K)^n - 1} \quad (15)$$

in (15), K is the interest rate and assumed 0.15 and n is the expected life-time for the component part of the proposed system and assumed 20 yrs.

And total cost of the system can be expressed as [23]:

$$\dot{c}_{tot} = \Sigma \dot{c}_p \quad (16)$$

The relative cost difference (r_i) for the i^{th} system is calculated as [23]:

$$r_i = \frac{(c_{P,i} - c_{F,i})}{c_{F,i}} \quad (17)$$

To evaluate the relative importance of each component of the system from the exergoeconomic view point, the exergoeconomic factor is defined as follows [23]:

$$f_i = \frac{\dot{Z}_i}{(\dot{Z}_i + \dot{c}_{D,i})} \quad (18)$$

All available costs data are for different years and should be updated to recent costs so, the recent costs estimated from reference year as following equation [23]:

$$Cost\ of\ target\ year = cost\ of\ reference\ yare \times \frac{cost\ index\ of\ target\ year}{cost\ index\ of\ reference\ year} \quad (19)$$

The NPV factor is one the most important economic index that represent the profitably and payback period and it should be considered in economic analysis of proposed system. The NPV exchange the future prices by considered interest rate to present prices which is led to indicate the economic performance of designed system and calculated by following expression [24]:

$$NPV_n = -TCI + \sum_{n=0}^{n} Y(1+i)^{-n} \quad (20)$$

where i is the interest rate that considered as 15% and n is the economic lifetime of the proposed system which is assumed 20 years. Also, Y represents the net cash flow at the end of nth year that is presented as follows [24]:

$$Y = AI - \left(C^{O\&M} + C_f\right) \quad (21)$$

AI is the annual income, $C^{O\&M}$ is the operation/maintenance costs, and C_f is the fuel cost. These terms are defined as follows [23]:

$$AI = c_{elec} \times t_{year} \times \dot{W}_{net} \quad (22)$$

$$C^{O\&M} = 0.06 \times PEC \quad (23)$$

$$C_f = 0 \quad (24)$$

The payback period defined as the minimum time that NPV become greater than zero and estimated as [24]:

$$PP = min\{n: NPV(n) > 0\} \quad (25)$$

The cost-balance, cost function and auxiliary equations of each component are presented at Table 4.

Table 4. Cost function, cost balance and auxiliary equations for Case-I components.

Components	Cost functions	Cost balance	Auxiliary equations
Expansion valve 1	$\mathrm{PEC}_{\mathrm{EV},1} = 114.5 \times \dot{m}_1$	$\dot{C}_1 + \dot{Z}_{\mathrm{EV},1} = \dot{C}_2$	–
Separator	$\mathrm{PEC}_{\mathrm{Sep}} = 0$	$\dot{C}_2 + \dot{Z}_{\mathrm{Sep}} = \dot{C}_3 + \dot{C}_4$	$c_4 = c_3$
Steam turbine	$\mathrm{PEC}_{\mathrm{ST}} = 3880.5 \times \dot{W}_{\mathrm{ST}}^{0.7} \left(1 + \left(\frac{0.05}{0.92-\eta_{\mathrm{is,ST}}}\right)^3\right)\left(1 + 5 \times 2.71^{\frac{(T_3-866)}{10.42}}\right)$	$\dot{C}_3 + \dot{Z}_{\mathrm{ST}} = \dot{C}_5 + \dot{C}_{\mathrm{W,ST}}$	$c_3 = c_5$
Condenser 1	$\mathrm{PEC}_{\mathrm{Cond},1} = 8000\left(\frac{A_{\mathrm{Cond},1}}{100}\right)^{0.6}$	$\dot{C}_5 + \dot{C}_{14} + \dot{Z}_{\mathrm{Cond},1} = \dot{C}_6 + \dot{C}_{15}$	$c_{14} = 0, c_5 = c_6$
Mixer	$\mathrm{PEC}_{\mathrm{Mixer}} = 0$	$\dot{C}_6 + \dot{C}_8 + \dot{Z}_{Mixer} = \dot{C}_9$	–
Expansion valve 2	$\mathrm{PEC}_{\mathrm{EV},2} = 114.5 \times \dot{m}_7$	$\dot{C}_7 + \dot{Z}_{\mathrm{EV},2} = \dot{C}_8$	–
Vapor generator	$\mathrm{PEC}_{\mathrm{VG}} = 17500\left(\frac{A_{\mathrm{VG}}}{100}\right)^{0.6}$	$\dot{C}_4 + \dot{C}_{13} + \dot{Z}_{\mathrm{VG}} = \dot{C}_{10} + \dot{C}_7$	$c_4 = c_7$
Turbine	$\mathrm{PEC}_{\mathrm{Tur}} = 4750\left(\dot{W}_{\mathrm{Tur}}\right)^{0.75}$	$\dot{C}_{10} + \dot{Z}_{\mathrm{Tur}} = \dot{C}_{11} + \dot{C}_{\mathrm{W,Tur}}$	$c_{10} = c_{11}$
Condenser 2	$\mathrm{PEC}_{\mathrm{Cond},2} = 8000\left(\frac{A_{\mathrm{Cond},2}}{100}\right)^{0.6}$	$\dot{C}_{11} + \dot{C}_{16} + \dot{Z}_{\mathrm{Cond},2} = \dot{C}_{12} + \dot{C}_{17}$	$c_{16} = 0, c_{11} = c_{12}$
Pump	$\mathrm{PEC}_{\mathrm{Pump}} = 200\left(\dot{W}_{\mathrm{Pump}}\right)^{0.65}$	$\dot{C}_{12} + \dot{Z}_{\mathrm{Pump}} + \dot{C}_{\mathrm{W,Pump}} = \dot{C}_{13}$	–

3.4. Performance criteria

In this section, the performance criteria of the proposed cases of study have been studied. The net power production at the ORC subsystem and whole system is calculated as:

$$\dot{W}_{Net,ORC} = \dot{W}_{Tur} - \dot{W}_{Pump} \tag{26}$$

$$\dot{W}_{Net} = (\dot{W}_{ST} + \dot{W}_{Tur}) - \dot{W}_{Pump} \tag{27}$$

Also, the energy and exergetic efficiency of ORC subsystem and whole system are estimated from following equations:

$$\eta_{en,ORC} = \frac{\dot{W}_{Net,ORC}}{\dot{m}_{(4)} \times (h_{(4)} - h_{(7)})} \tag{28}$$

$$\eta_{en} = \frac{\dot{W}_{Net}}{\dot{m}_{(1)} \times (h_{(1)} - h_{(9)})} \tag{29}$$

$$\eta_{ex,ORC} = \frac{\dot{W}_{Net,ORC}}{\dot{E}_{(4)} - \dot{E}_{(7)}} \tag{30}$$

$$\eta_{ex} = \frac{\dot{W}_{Net}}{\dot{E}_{(1)} - \dot{E}_{(9)}} \tag{31}$$

4. Results and discussion

4.1. Results validation

The mass, energy, exergy, and exergoeconomic analysis are applied to all study cases via ESS code. Before presenting the obtained results, the flash separator tank's simulation is validated with Wang et al. [25]. The flash separator tank simulation's results are compared with Ref. [25], and illustrated in Fig. 2, which are in good accuracy and validated the conducted simulation.

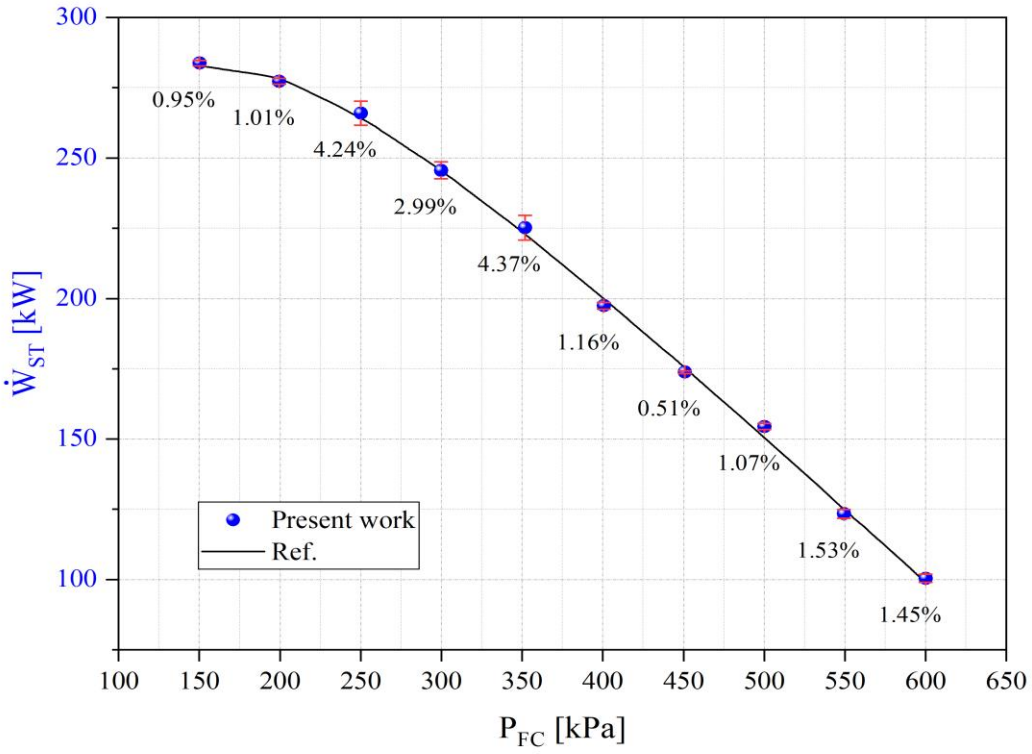

Fig. 2. The validation of flash cycle simulation with Wang et al. [25].

4.2. Parametric study

This section studies the effect of zeotropic solution's mass fraction and vapor generator evaporation temperature variation on the ORC and proposed system exergy destruction, net output power, energy, exergetic efficiencies, and the payback period.

4.2.1. The ORC subsystem and proposed system exergy destruction

The effect of zeotropic mixture mass fraction and vapor generator evaporation temperature on the ORC and proposed system exergy destruction are shown in Figs. 3a and 3b, individually. The exergy destruction of the ORC subsystem increases when the mass fraction of neopentane in the zeotropic mixture reaches 0.1. Then decreases it until the fraction of 0.6, and finally, the exergy destruction increases for the mass fraction of higher than 0.6. This ORC exergy demolition is attended by deliberate various vapor generator evaporation temperatures. Besides, growing the vapor generator evaporation temperature decreases the ORC subsystem exergy devastation, and this flow is acted for the different mass fractions. So, the mass fraction of 0.1 and 365 K evaporation temperature present the maximum exergy destruction, and the 0.6 and 381 K mass fraction and evaporation contribute the minimum exergy destruction for the ORC subsystem. The total exergy destruction of the proposed system trend with zeotropic solution's mass fraction and vapor generator evaporation temperature is the same with the ORC subsystem. But, the minimum exergy destruction is presented by mass fraction of 0.5, with the highest considered evaporation temperature. Comparing the ORC subsystem and proposed system exergy destruction variation with the zeotropic solution's mass fraction and vapor generator evaporation temperature demonstrates that these parameters influence the ORC subsystem exergy destruction higher than the system total exergy destruction. So that, the maximum and minimum exergy destruction dissimilarity in the ORC subsystem is about 33.79%, while in the total exergy destruction, this difference is about 17.6%.

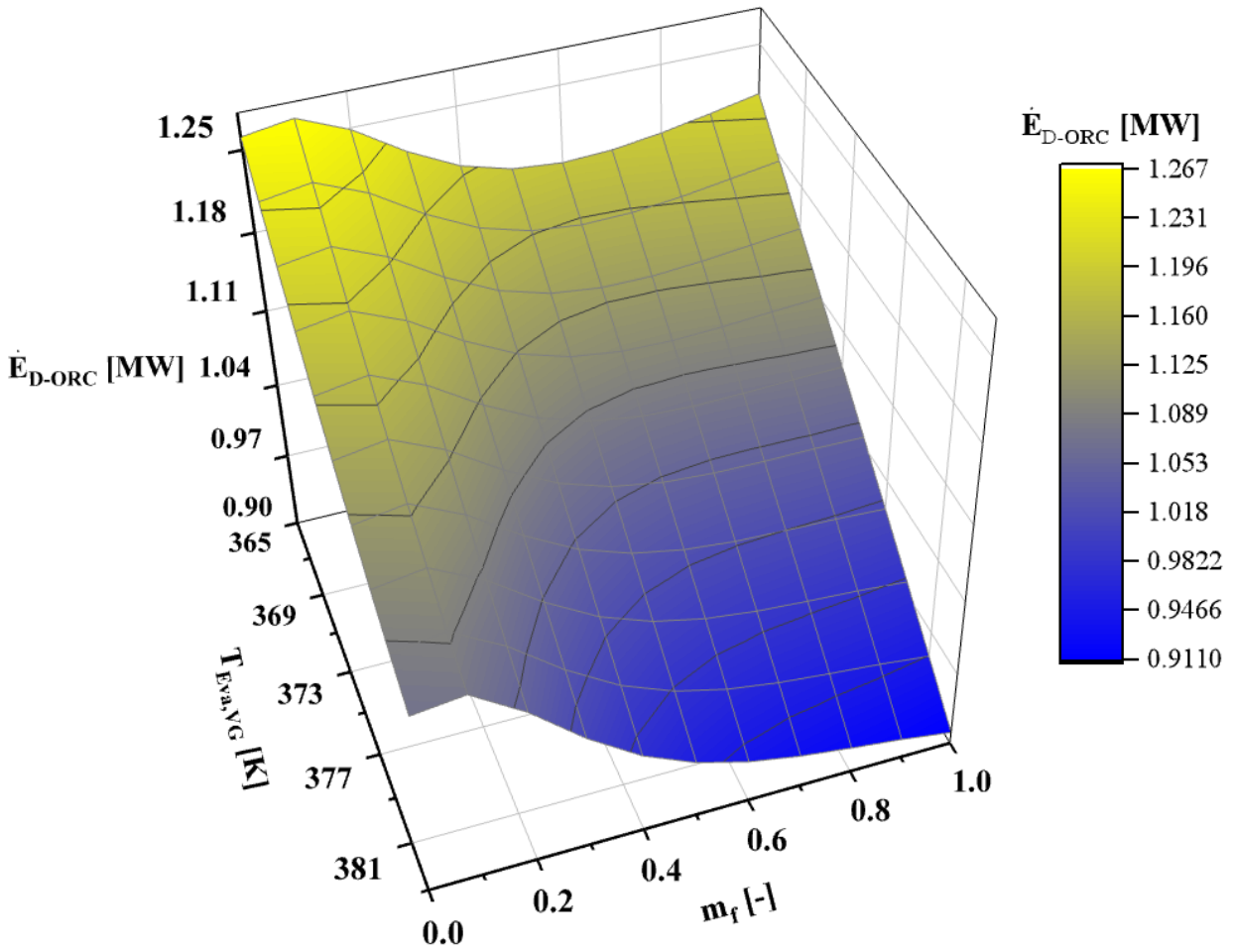

Fig. 3a. Effect of zeotropic solution's mass fraction on the ORC subsystem exergy destruction.

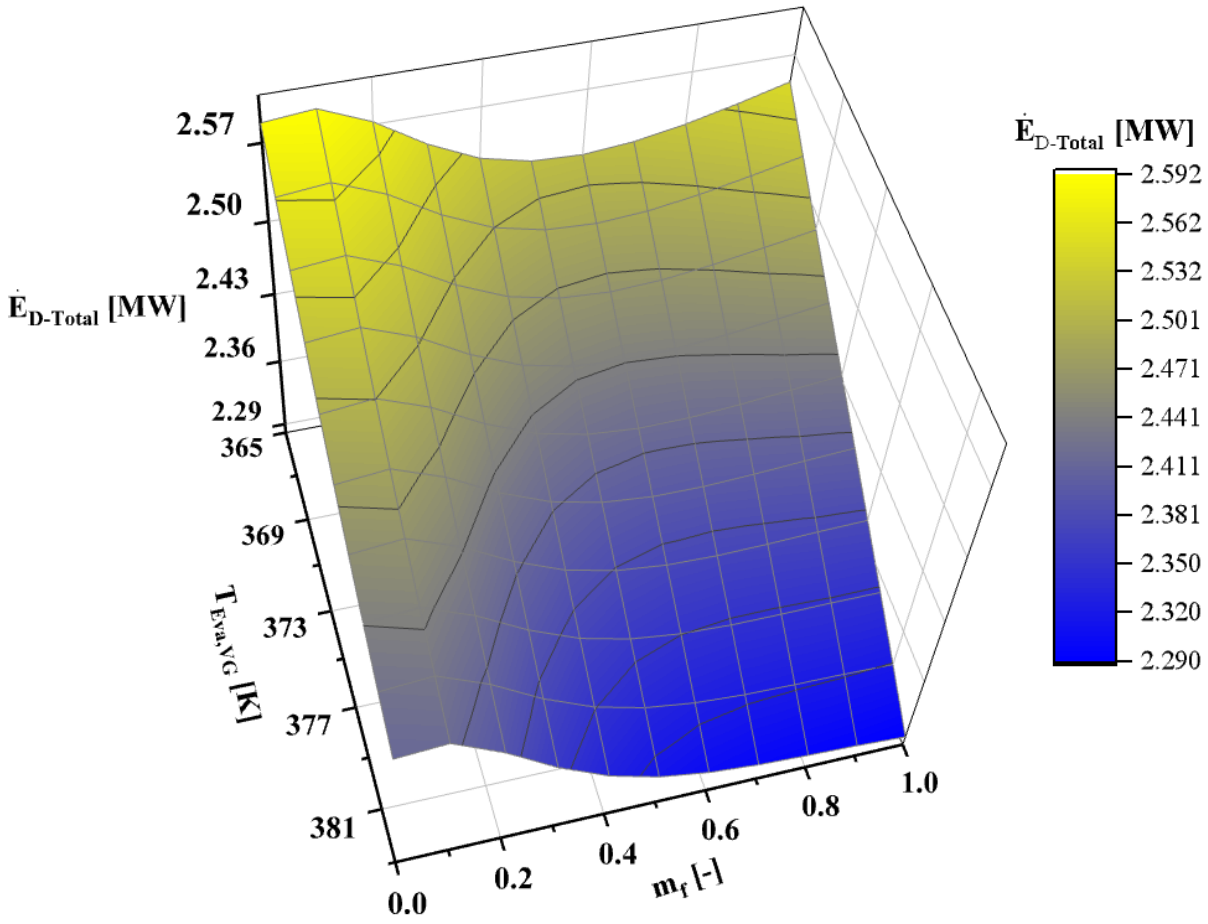

Fig. 3b. Effect of zeotropic solution's mass fraction on the proposed system exergy destruction.

4.2.2. The net output power

The net output power of the ORC subsystem, by assuming constant evaporation temperature in the vapor generator, first increases then decreases through the increasing of the Neopentane concentration. But the maximum net output power is presented by different mass fractions at different evaporation temperatures. At the evaporation temperature of 365 K, the maximum ORC subsystem net output power is generated at the mass fraction of 0.4. In comparison, at 381 K, the maximum net power is generated at the mass fraction of 0.1. On the other hand, increasing the vapor generator evaporation temperature at the different mass fractions presents different trends. So that the net power increases by increasing the evaporation temperature at the mass fraction of 0 to 0.1. While for higher mass fractions, increasing the evaporation temperature decreases the net power. The overall results of increasing the mass fraction and evaporation indicate that the maximum net power is presented at the mass fraction of 0.4 and 365 K evaporation temperature, and the minimum net power is presented by the mass fraction of 1 and 381 K evaporation temperature. The total net power of the proposed system at the constant evaporation temperature, by increasing the mass fraction of Neopentane in the zeotropic solution increases then decreases. But, the peak point of power generation at the various evaporation temperature is different and follows the ORC subsystem trend. Focusing on the obtained results demonstrates that the minimum net total output power belongs to the mass fraction of 1 and 381 K evaporation temperature. The maximum net output power is represented by the mass fraction of 0.4 and 365 K evaporation temperature. More details of mass fraction and evaporation temperature variation on net output power are shown in Figs. 4a and 4b.

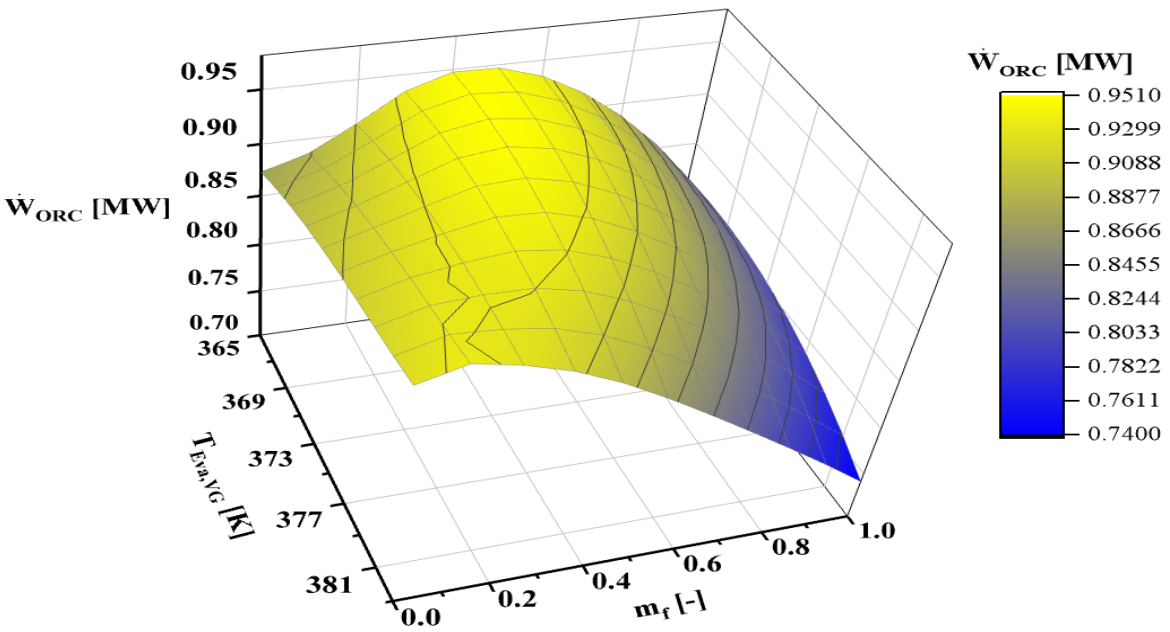

Fig. 4a. Effect of zeotropic solution's mass fraction on the ORC subsystem's net output power

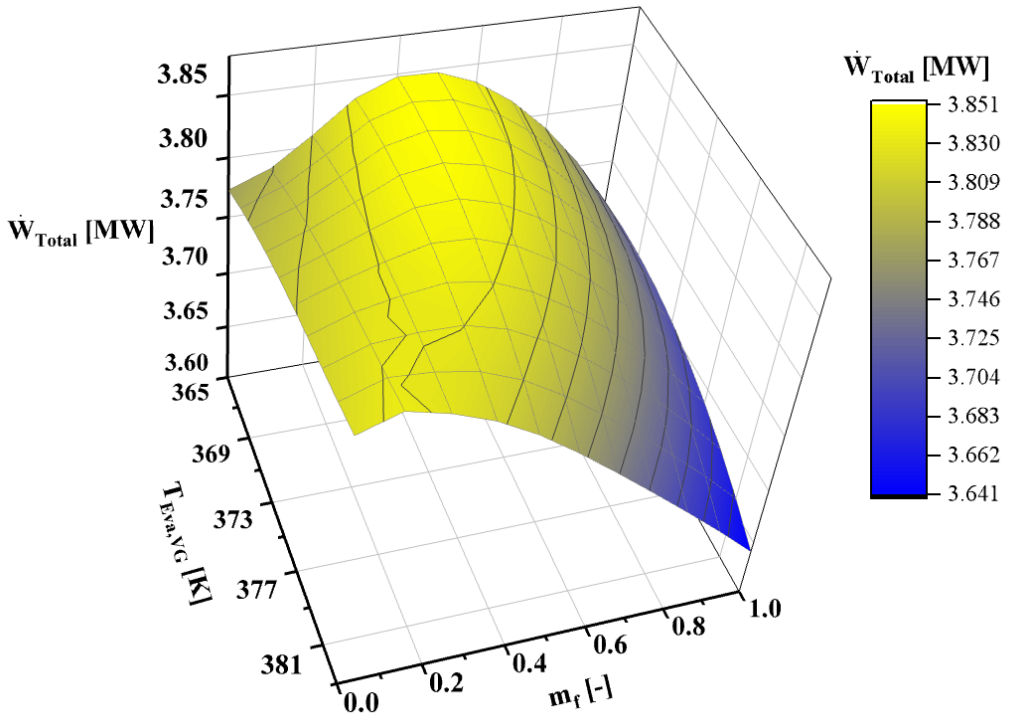

Fig. 4b. Effect of zeotropic solution's mass fraction on the proposed system total net output power.

4.2.3. Energy efficiency

The energy efficiency of the ORC subsystem at the constant evaporation temperature decreases by increasing the Neopentane mass fraction in the zeotropic solution to 0.1. Then, the energy efficiency increases by increasing the mass fraction until 0.6 and drops again for the higher mass fraction. This trend contains all considered evaporation temperature but, the second part of energy efficiency decline's slope decreases by increasing the evaporation temperature. Also, based on obtained results which are

illustrated in Fig. 5a, the maximum ORC subsystem's energy efficiency belongs to the mass fraction of 0.6 and 381 K evaporation temperature, and the mass fraction of 0.1 and evaporation temperature of 365 K presents the minimum energy efficiency. On the other hand, for constant mass fraction, increasing the vapor generator's evaporation temperature leads to improving the energy efficiency of the ORC subsystem. Hence, higher evaporation temperature presents higher energy efficiency. The overall analysis of mass fraction and evaporation temperature variation effect on the ORC subsystem's energy efficiency demonstrates the maximum, and the minimum energy efficiency belongs to mass fraction and evaporation temperature of 1 and 381 K, 0.1 and 365 K, respectively. Fig. 5b shows the effect of zeotropic solution mass fraction and vapor generation's evaporation temperature on the total energy efficiency of the proposed system. Increasing the Neopentane mass fraction in the zeotropic solution to 0.1 decreases the energy efficiency and improves it up to the mass fraction of 1, and this trend contains all evaporation temperatures. On the other hand, increasing the evaporation temperature in the vapor generator by assuming the constant mass fraction increases the total energy efficiency of the proposed system. Also, the maximum energy efficiency is presented by the mass fraction and evaporation temperature of 1 and 381 K, respectively. The minimum energy efficiency is obtained at the mass fraction of 0.1 and 365 K evaporation temperature.

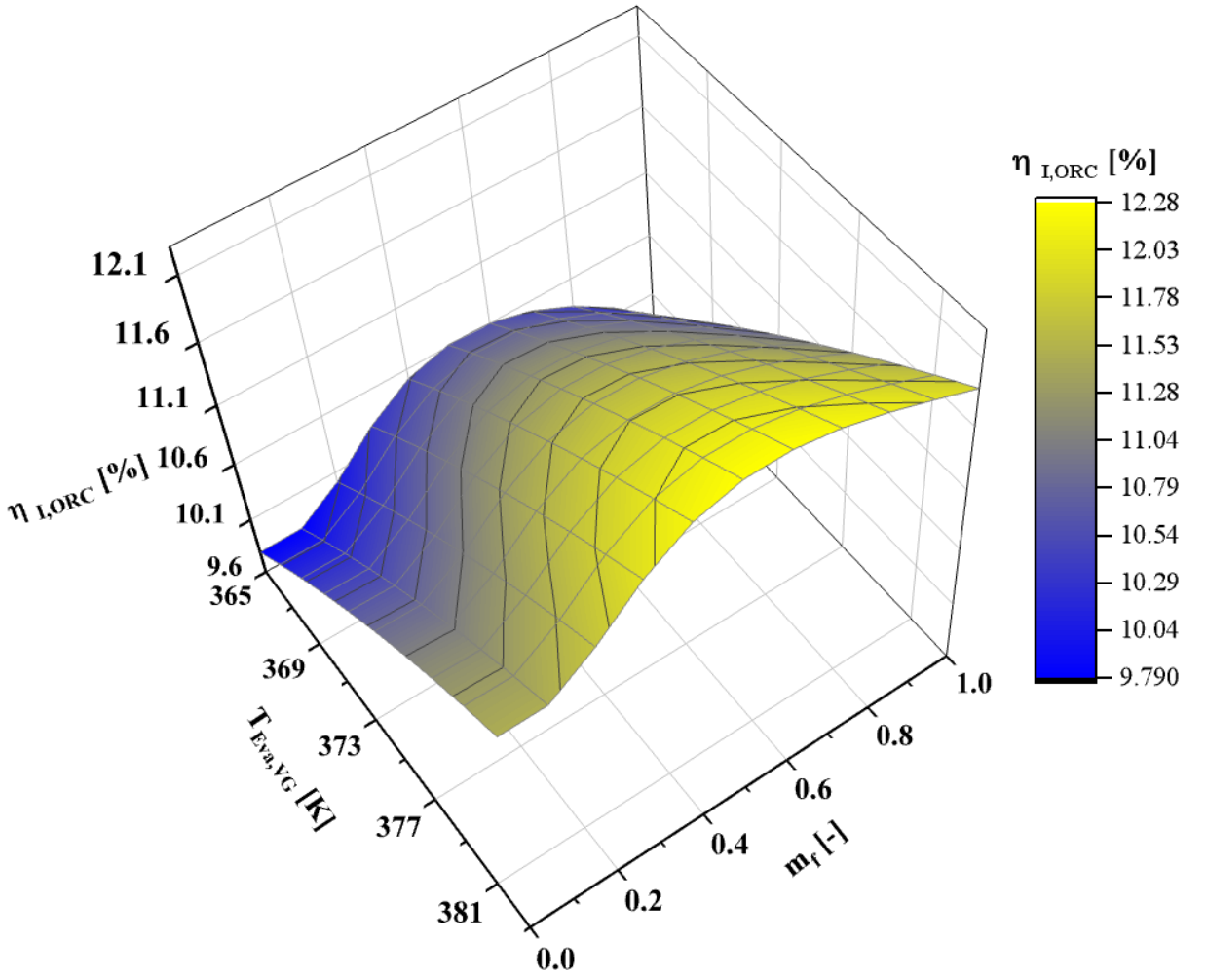

Fig. 5a. Effect of zeotropic solution's mass fraction on the ORC subsystem energy efficiency.

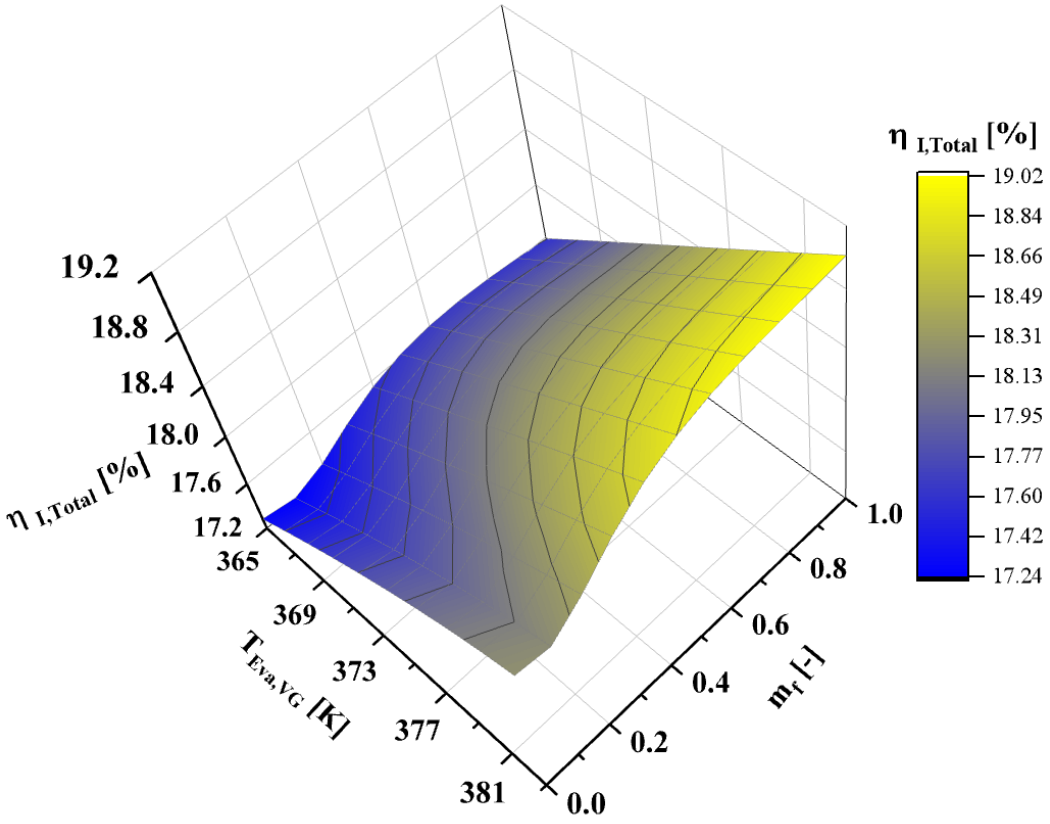

Fig. 5b. Effect of zeotropic solution's mass fraction on the total energy efficiency of proposed system.

4.2.4. Exergetic efficiency

Fig. 6a shows the effect of vapor generator temperature and zeotropic mixture mass fraction variation on the ORC subsystem exergetic efficiency. By assuming constant evaporation temperature in the vapor generator, the exergetic efficiency increases by increasing the Neopentane mass fraction of 0.5 then decreases for the higher mass fraction. This trend is performed for considered evaporation temperature dominance. Besides, for the constant mass fraction, the exergetic efficiency increases by increasing the evaporation temperature. This phenomenon is because the ORC subsystem's net power generation increases by increasing the mass fraction then decrease. Besides, the exergy destruction decreases by increasing the evaporation temperature for the constant mass fraction. On the other hand, the exergy destruction of the ORC subsystem first increases then reduces by increasing the mass fraction. So, overlapping the net output power trend with exergy destruction leads to obtaining the maximum exergetic efficiency of the ORC subsystem at the mass fraction of 0.5 and 381 K evaporation temperature. Also, the minimum ORC subsystem exergetic efficiency is presented by the mass fraction of 0 and 365 K evaporation temperature. The total exergetic efficiency trend is the same as the ORC subsystem's exergetic efficiency as shown in Fig. 6b, in which by increasing the mass fraction, the total exergetic efficiency increases until the mass fraction of 0.5 then decreases. Also, the total exergetic efficiency increases by increasing the vapor generator's evaporation temperature. The maximum and minimum total exergetic efficiency are presented by the same mass fraction and evaporation temperature. The differences between the ORC and total exergetic efficiency trend are that the slope of total exergetic efficiency variation with evaporation temperature is sharper than the slope of ORC subsystem exergetic efficiency, and the total exergetic efficiency declines slower than the ORC exergetic efficiency for the mass fraction of higher than 0.5.

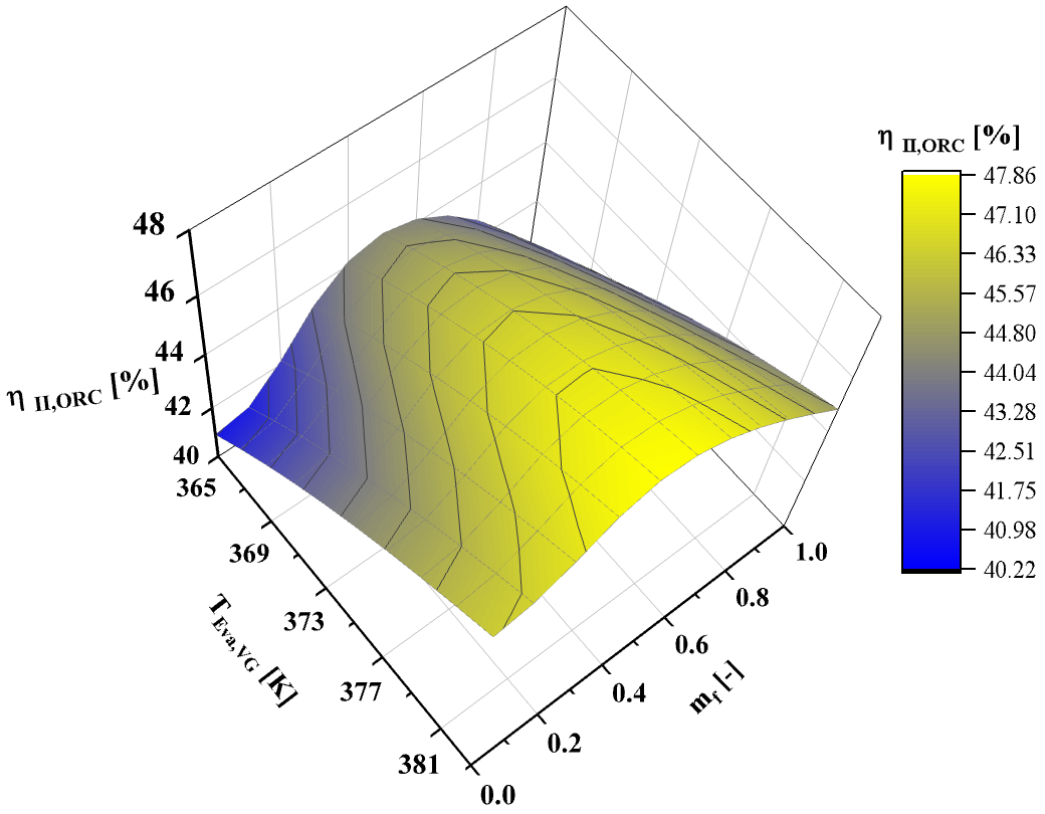

Fig. 6a. Effect of zeotropic solution's mass fraction on the ORC subsystem exergetic efficiency.

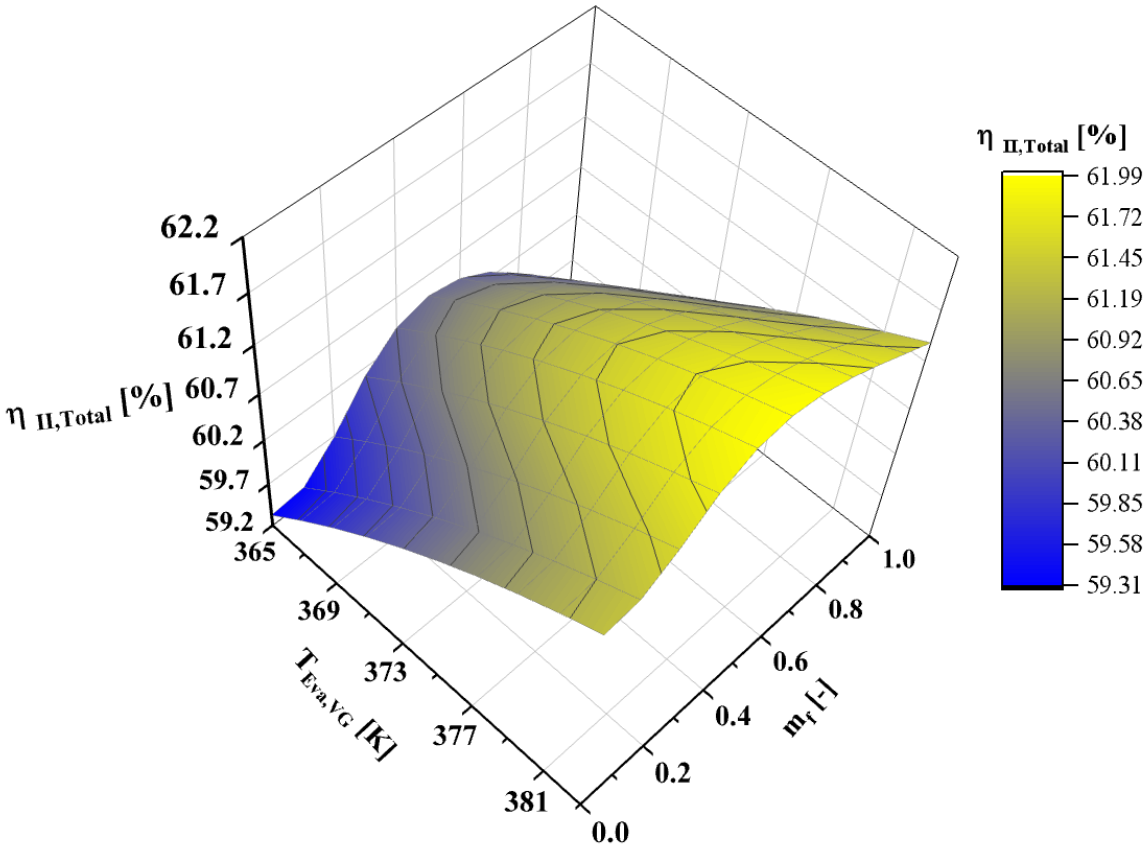

Fig. 6b. Effect of zeotropic solution's mass fraction on the total exergetic efficiency of the proposed system.

4.2.5. The payback periods

The variation of the payback period with the mass fraction of the zeotropic mixture and the variation of the vapor generator temperature is shown in Figure 7. The payback period for different evaporation temperature decreases with growing the Neopentane portion in the zeotropic mass fraction then increases. For the higher evaporation temperature, the payback period decline slope decreases, and the rising slope increases. Also, the turning-point of the payback trend is performed at the lower mass fraction for higher evaporation temperature. On the other hand, increasing the evaporation temperature decreases the payback period for the constant mass fraction. But this trend is corroborated until the mass fraction of 0.2. Then, for the higher mass fraction, the payback period first declines and then increases by growing the evaporation temperature. These decline and rise are acted in the higher slope for the extreme mass fraction. The overall results of this section indicate the minimum payback period belongs to the mass fraction of 0.4 with 365 K evaporation temperature, and the maximum payback period is bestowed to the mass fraction of 1 and 381 K evaporation temperature.

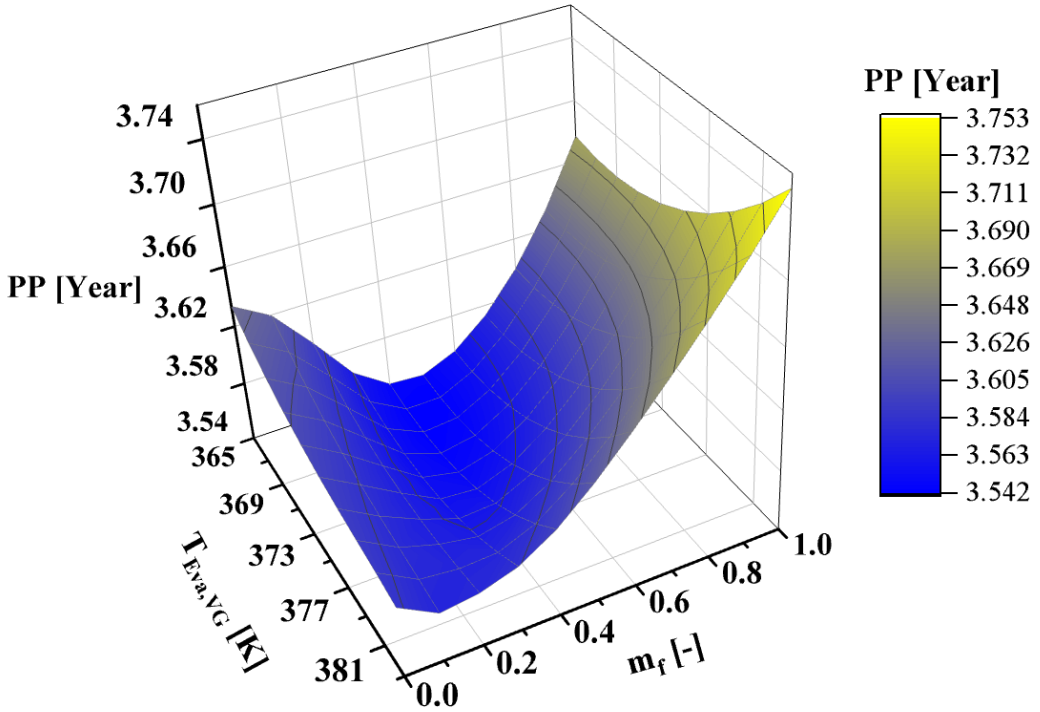

Fig. 7. Effect of zeotropic solution's mass fraction on the proposed system payback period.

4.3. The Sankey diagrams

The Sankey diagram presents useful data about the system's exergy flow. Hence, the Sankey diagram of proposed configurations is illustrated. Fig. 8 shows the Sankey diagram of the proposed system. The geofluid carries 6752 kW exergy flow and enters the expansion valve, which leads to 412 kW exergy destruction. Then, the geofluid enters the flash separator tank and provides 3392 kW exergy for the steam turbine. In the steam turbine, 2900 kW power is generated, and 493 kW exergy flow is destructed. On the other hand, 2051 kW exergy flow enters to vapor generator. The vapor generator presents 552 kW exergy destruction, and the rest of the exergy is transferred to the ORC subsystem and second expansion valve. In the ORC subsystem, the vapor generator provides 1157 kW exergy flow for the ORC turbine. The ORC turbine generates 1000 kW power and destroys 157 kW exergy flow. The overall Sankey diagram of the case I indicate that the vapor generator, first expansion valve, and steam turbine contain the highest exergy destruction. Also, the total exergy destruction of the proposed system is obtained by about 2297 kW, and 47 kW exergy flow brine to underground.

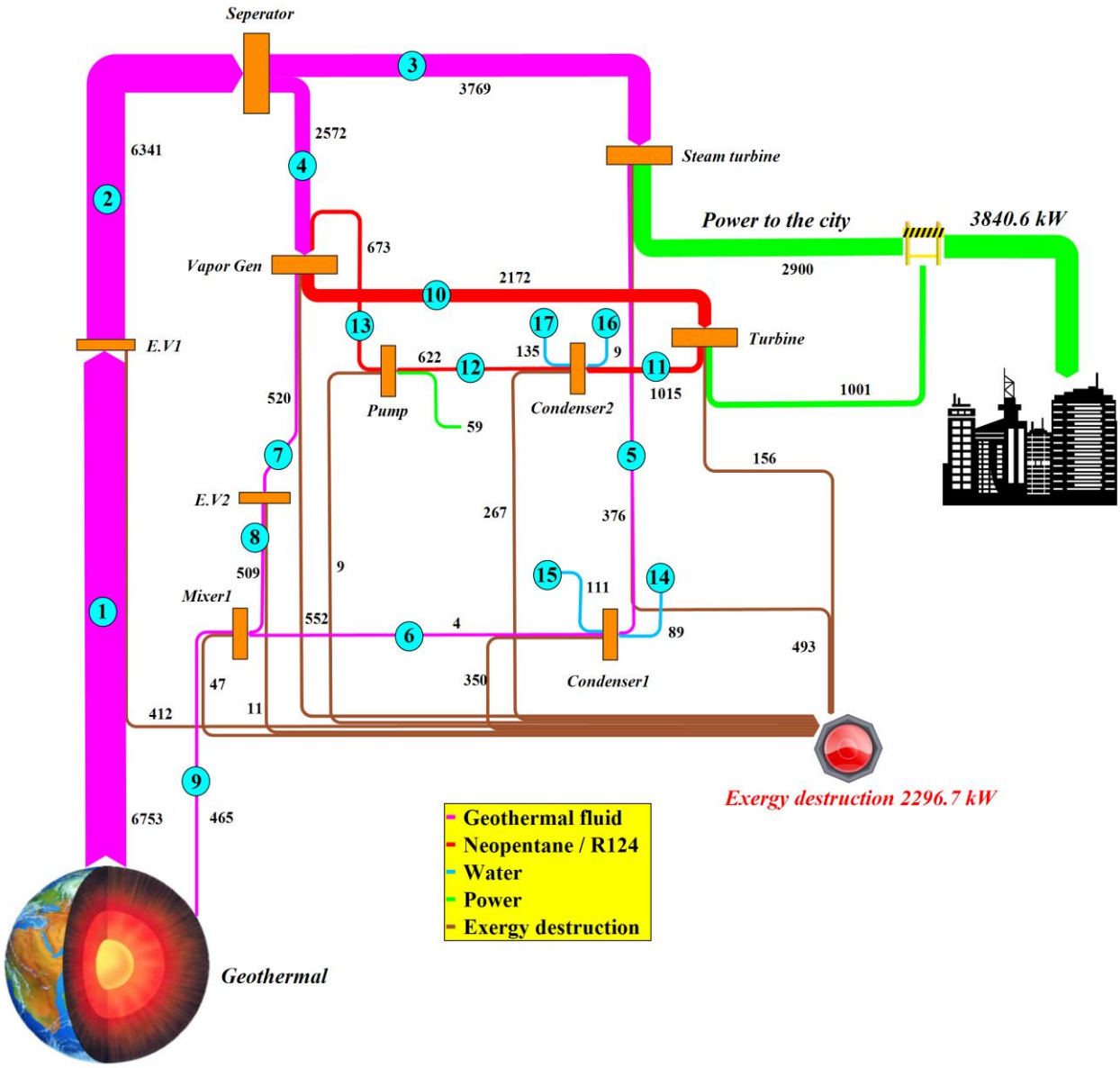

Fig. 8. The Sankey diagram of the proposed system.

4.4. The Net Present Value estimation

The NPV estimation leads to evaluating the proposed system's payback period and profitably in the designed lifetime. Also, it shows the financial roadmap of the system's economic performance. Hence, in this section, the NPV of the proposed system is estimated for three different geofluid and electric sale prices. Fig. 9 shows the NPV of the proposed system for the three different scenarios of geofluid and electricity sale prices. In the first scenario the geofluid and electricity sale prices is considered 1.3 $/GJ and 0.09 $/kWh, respectively. At these prices, the proposed system's payback period is obtained by about 3.55 years and the system presents 6.14 M$ net profit. At the second scenario the geofluid and electricity sale prices are assumed 1.9 $/GJ and 0.07 $/kWh, respectively. Considering these prices lead to obtain the payback period longer than the system's lifetime. Subsequently, at the 20 years system life time, the proposed system does not present any profit and provides 6.03 M$ lost. In the third scenario, the geofluid price is considered 1.3 $GJ and the electricity sale price is assumed 0.11 $/kWh. At this sale and incoming prices scenario, the payback period is obtained about 2.73 years with 9.50 M$ net profit during the 20 years system's life time. Also, the comparison of first and third scenarios results demonstrates that increasing the electricity sale prices about 22% leads to decreasing the payback period by about 23% and presents 54.7% more net profit, which is considerable progress in the system viability.

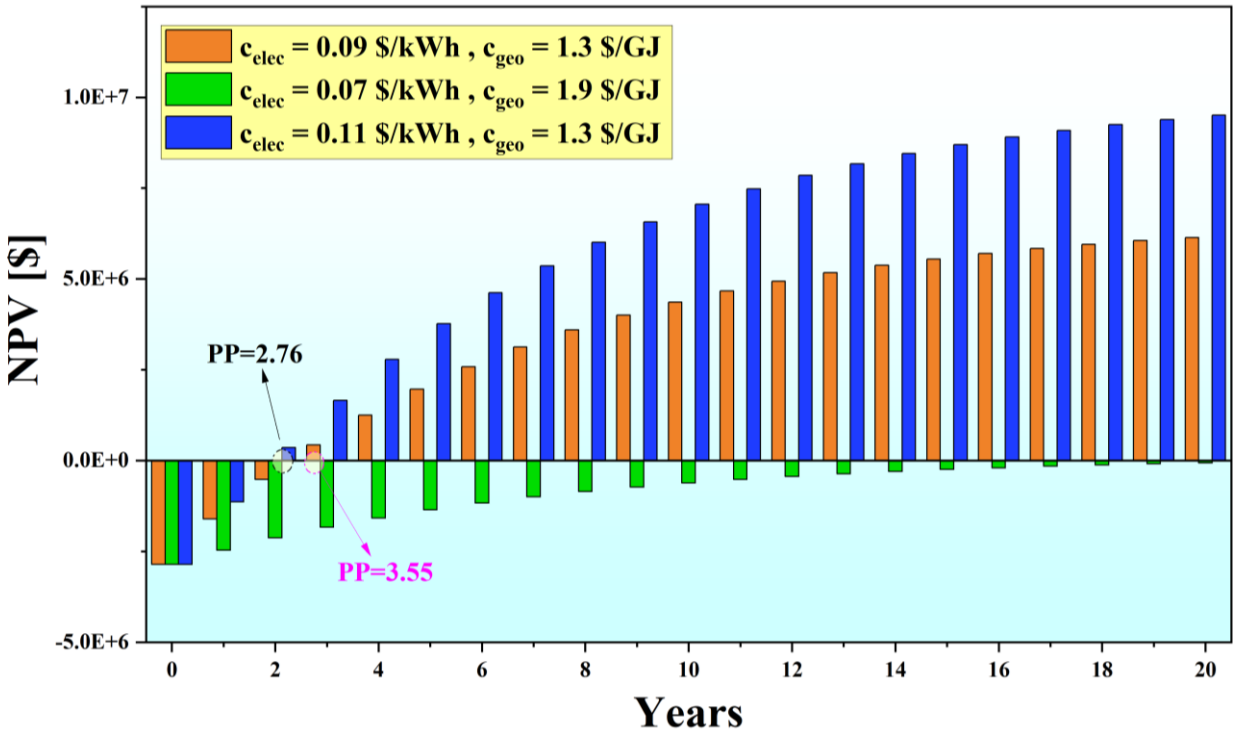

Fig. 9. The NPV of proposed system for three different price's scenarios.

5. Optimization

Comprehensive energy, exergy, and exergoeconomic analysis have been performed to evaluate the proposed system performance. The proposed system presents 3841 kW net power with 61.09% exergetic efficiency, and by considering the 1.3 $/GJ geofluid price and 0.09 $/kWh electricity sale price, the payback period is obtained about 3.55 years at the base condition of system operation. Hence, a multi-objective optimization based on the MOPSO method is conducted to obtain the optimum condition of system performance. The separator inlet pressure, ORC subsystem vapor generator temperature, and the zeotropic mixture mass fraction are selected as the decision-maker parameters. The payback period with exergetic efficiency is considered the cost function of optimization. Applying the MOPSO method to the proposed system leads to performing the Pareto-frontier of the optimum states, in which the scatter distributions of the decision-maker parameters are shown in Fig. 10. Then, the LINMAP code is applied to the Pareto-frontier to select the best optimum point. The LINMAP code result indicates that 62.15% and 3.26 years are the best optimum states of the proposed system's exergetic efficiency and payback period, respectively. Also, the optimization results are presented in Fig. 11 with more details.

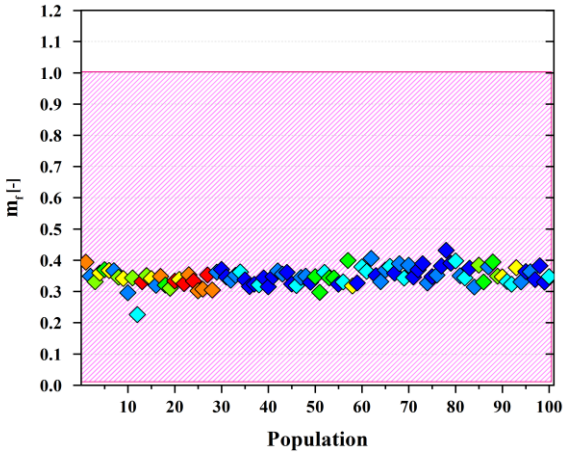

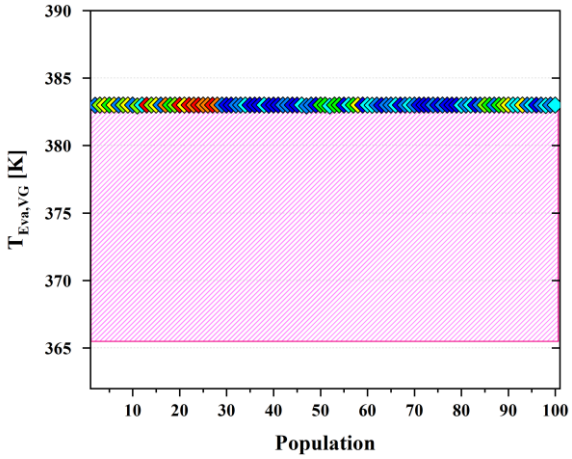

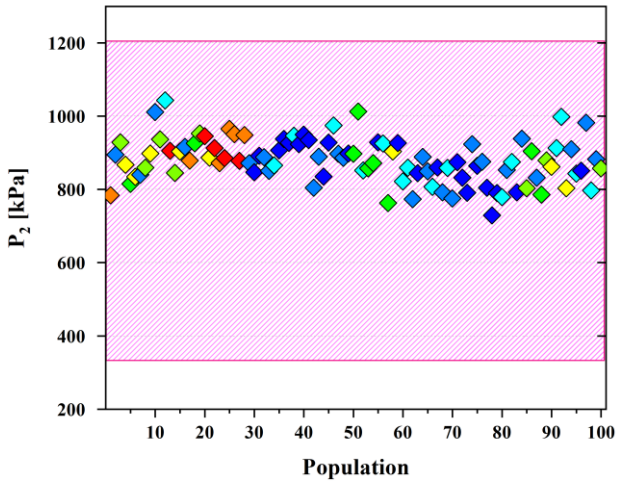

Fig. 10. The scatter distributions of the decision-maker parameters.

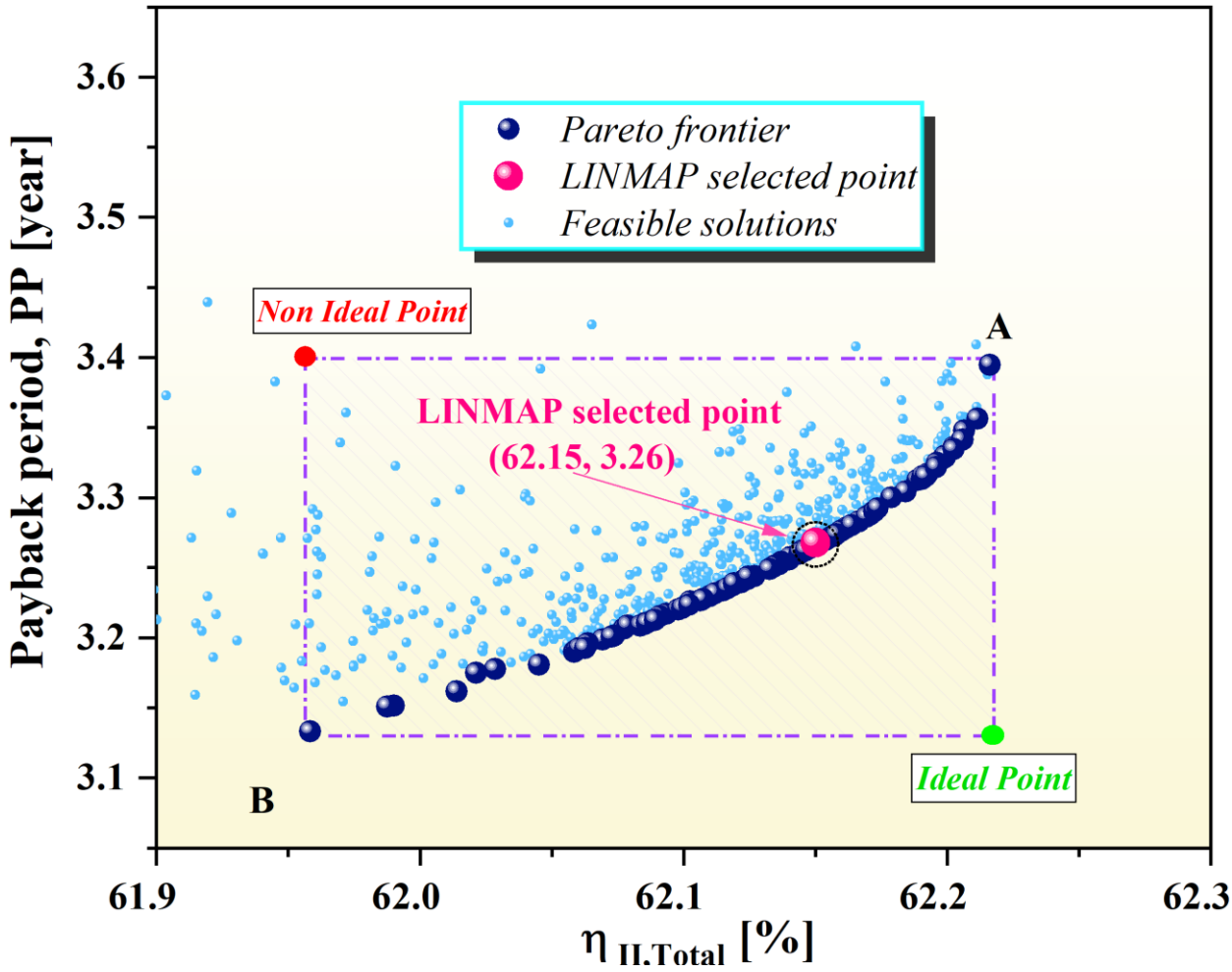

Fig. 11. The Pareto-frontier and optimization results.

6. Conclusion

In this paper, a geothermal power system was proposed to generate power. Also, an ORC subsystem with the zeotropic working fluid was employed to recover the geothermal system waste energy and generate more power. Comprehensive mass, energy, exergy, and exergoeconomic analysis were applied to evaluate the proposed system. Then, a parametric study was performed to study the effect of vapor generation and the zeotropic mass mixture's mass

fraction on the main performance criteria of the proposed system. The net present value was estimated for three different price scenarios to evaluate the proposed system's exergoeconomic performance. Finally, a multi-objective optimization based on the MOPSO method was applied to obtain the optimum condition of the proposed system performance. All conducted studies led to the following conclusions:

- The vapor generator, steam turbine, and expansion valve include the highest exergy destruction among the employed units in the proposed system.
- Increasing the vapor generator operational temperature decreases the exergy destruction for all zeotropic mixture mass fractions.
- Increasing the vapor generator evaporation temperature increases the net output power in the lower mass fraction while, for the mass fraction of more than 0.1 the net power generation decreases. So that, the maximum net power is presented by the mass fraction of 0.5 and 365 K evaporation temperature.
- The evaporation temperature's rise improves the thermal and exergetic efficiencies. Specially the ORC subsystem exergetic efficiency.
- Increasing the electricity sale price from 0.09 $/kWh to 0.11 $/kWh by assuming constant geofluid price improves the payback and system profit during the designed lifetime considerably.
- Applying the multi-objective optimization improves the system payback period and exergetic efficiency by about 8.14% and 1.06 compare to base condition, respectively.

For future work, the performance and improvement potential of each component of the organic flash Rankine cycle (ORFC) can be investigated by conventional exergy/exergoeconomic and advanced exergy/exergoeconomic analysis.

REFERENCES

[1] G. Shu, L. Liu, H. Tian, H. Wei, and G. Yu, "Parametric and working fluid analysis of a dual-loop organic Rankine cycle (DORC) used in engine waste heat recovery," *Applied Energy*, vol. 113, pp. 1188–1198, 2014.

[2] M. Malik, I. Dincer, and M. A. Rosen, "Development and analysis of a new renewable energy-based multi-generation system," *Energy*, vol. 79, pp. 90–99, 2015.

[3] J. Song, P. Loo, J. Teo, and C. N. Markides, "Thermo-economic optimization of organic Rankine cycle (ORC) systems for geothermal power generation: A comparative study of system configurations," *Frontiers in Energy Research*, vol. 8, p. 6, 2020.

[4] F. A. Boyaghchi and P. Heidarnejad, "Thermoeconomic assessment and multi objective optimization of a solar micro CCHP based on Organic Rankine Cycle for domestic application," *Energy conversion and Management*, vol. 97, pp. 224–234, 2015.

[5] M. Kanoglu and A. Bolatturk, "Performance and parametric investigation of a binary geothermal power plant by exergy," *Renewable Energy*, vol. 33, no. 11, pp. 2366–2374, 2008.

[6] S. J. Zarrouk and M. H. Purnanto, "Geothermal steam-water separators: Design overview," *Geothermics*, vol. 53, pp. 236–254, 2015.

[7] C. Luo, L. Huang, Y. Gong, and W. Ma, "Thermodynamic comparison of different types of geothermal power plant systems and case studies in China," *Renewable energy*, vol. 48, pp. 155–160, 2012.

[8] M. Yari, "Exergetic analysis of various types of geothermal power plants," *Renewable energy*, vol. 35, no. 1, pp. 112–121, 2010.

[9] A. D. Pasek, T. A. F. Soelaiman, and C. Gunawan, "Thermodynamics study of flash–binary cycle in geothermal power plant," *Renewable and Sustainable Energy Reviews*, vol. 15, no. 9, pp. 5218–5223, 2011.

[10] F. Musharavati, S. Khanmohammadi, and A. Pakseresht, "A novel multi-generation energy system based on geothermal energy source: Thermo-economic evaluation and optimization," *Energy Conversion and Management*, vol. 230, p. 113829, 2021.

[11] A. H. Mosaffa and A. Zareei, "Proposal and thermoeconomic analysis of geothermal flash binary power plants utilizing different types of organic flash cycle," *Geothermics*, vol. 72, pp. 47–63, 2018.

[12] M. H. Seyyedvalilu, V. Zare, and F. Mohammadkhani, "Comparative thermoeconomic analysis of trigeneration systems based on absorption heat transformers for utilizing low-temperature geothermal energy," *Energy*, vol. 224, p. 120175, 2021.

[13] Z. Guzović, B. Majcen, and S. Cvetković, "Possibilities of electricity generation in the Republic of Croatia from medium-temperature geothermal sources," *Applied energy*, vol. 98, pp. 404–414, 2012.

[14] J. Li, Z. Ge, Y. Duan, Z. Yang, and Q. Liu, "Parametric optimization and thermodynamic performance comparison of single-pressure and dual-pressure evaporation organic Rankine cycles," *Applied energy*, vol. 217, pp. 409–421, 2018.

[15] Z. Ge, J. Li, Q. Liu, Y. Duan, and Z. Yang, "Thermodynamic analysis of dual-loop organic Rankine cycle using zeotropic mixtures for internal combustion engine waste heat recovery," *Energy*

conversion and management, vol. 166, pp. 201–214, 2018.
[16] W. Li, X. Feng, L. J. Yu, and J. Xu, "Effects of evaporating temperature and internal heat exchanger on organic Rankine cycle," *Applied Thermal Engineering*, vol. 31, no. 17–18, pp. 4014–4023, 2011.
[17] X. D. Wang and L. Zhao, "Analysis of zeotropic mixtures used in low-temperature solar Rankine cycles for power generation," *Solar Energy*, vol. 83, no. 5, pp. 605–613, 2009.
[18] L. Zhao and J. Bao, "Thermodynamic analysis of organic Rankine cycle using zeotropic mixtures," *Applied Energy*, vol. 130, pp. 748–756, 2014.
[19] A. Sohani, H. Sayyaadi, and M. Zeraatpisheh, "Optimization strategy by a general approach to enhance improving potential of dew-point evaporative coolers," *Energy Conversion and Management*, vol. 188, pp. 177–213, 2019.
[20] T. Parikhani, J. Jannatkhah, A. Shokri, and H. Ghaebi, "Thermodynamic analysis and optimization of a novel power generation system based on modified Kalina and GT-MHR cycles," *Energy Conversion and Management*, vol. 196, 2019, doi: 10.1016/j.enconman.2019.06.018.
[21] H. Rostamzadeh, M. Ebadollahi, H. Ghaebi, and A. Shokri, "Comparative study of two novel micro-CCHP systems based on organic Rankine cycle and Kalina cycle," *Energy conversion and management*, vol. 183, pp. 210–229, 2019.
[22] Y. A. Cengel, M. A. Boles, and M. Kanoglu, *Thermodynamics: an engineering approach*, vol. 5. McGraw-hill New York, 2011.
[23] A. Bejan, G. Tsatsaronis, and M. J. Moran, *Thermal design and optimization*. John Wiley & Sons, 1995.
[24] F. Hamrang, A. Shokri, S. M. Mahmoudi, B. Ehghaghi, and M. A. Rosen, "Performance Analysis of a New Electricity and Freshwater Production System Based on an Integrated Gasification Combined Cycle and Multi-Effect Desalination," *Sustainability*, vol. 12, no. 19, p. 7996, 2020.
[25] J. Wang, J. Wang, Y. Dai, and P. Zhao, "Thermodynamic analysis and optimization of a flash-binary geothermal power generation system," *Geothermics*, vol. 55, pp. 69–77, 2015.
[26] M. Zhang, A. Timoshin, E. A. Al-Ammar, M. Sillanpaa, and G. Zhang, "Power, cooling, freshwater, and hydrogen production system from a new integrated system working with the zeotropic mixture, using a flash-binary geothermal system," Energy, 2023.